Combustion and Flame 199 (2019) 122–130

Contents lists available at ScienceDirect

Combustion and Flame

journal homepage: www.elsevier.com/locate/combustflame

The effect of butanol isomers on the formation of carbon particulate matter in fuel-rich premixed ethylene flames

Carmela Russo[a], Andrea D'Anna[b], Anna Ciajolo[a], Mariano Sirignano[b,*]

[a] Istituto di Ricerche sulla Combustione, Consiglio Nazionale delle Ricerche, P.le Tecchio 80, 80125 Napoli, Italy
[b] Dipartimento di Ingegneria Chimica, dei Materiali e della Produzione Industriale – Università degli Studi di Napoli Federico II, P.le Tecchio 80, 80125 Napoli, Italy

ARTICLE INFO

Article history:
Received 4 July 2018
Revised 28 August 2018
Accepted 19 October 2018
Available online 28 October 2018

Keywords:
Butanol
Biofuels
Soot
Nanoparticles
Premixed flames

ABSTRACT

The effect of the butanol isomers on carbon particulate matter formation was studied by substituting up to 20% of the total carbon of ethylene, fed to premixed flames with different equivalence ratios, with the four butanol isomers. Soot and condensed-phase nanostructures were tracked by means of particle size distribution (PSD) measurements and laser induced emission spectroscopy, namely fluorescence and incandescence. Butanol isomers, especially t-butanol, significantly reduced the total amount and the size of the soot particles, whereas a negligible effect was detected on condensed-phase nanostructures. PSDs were measured along with the aromaticity and functionalities of the carbon particulate matter thermophoretically sampled in the highest equivalence ratio condition. No significant differences were found among the different butanol isomers neither in the soot aggregate size, as measured by size exclusion chromatography, nor in the aromaticity, as evaluated by Raman and UV–vis spectroscopy, of the particulate matter. Conversely, FTIR analysis showed that carbon particulate matter produced from 1-butanol and t-butanol-doped flames contained larger amounts of oxygen in form of C=O, C–O–C and OH functionalities. However, most of the differences in the oxygen functionalities disappeared after dichloromethane (DCM) treatment, suggesting that these oxygenated moieties belong to the condensed-phase nanostructures, soluble in DCM, rather than to soot particles.

1. Introduction

Biofuels as alcohols are an important alternative to fossil fuels, especially for internal combustion engines, because their use reduces not only the net production of carbon dioxide emissions, but also the emissions of health dangerous pollutants, such as carbon particulate matter (PM) [1,2]. The PM mass concentration is no longer the only emission parameter to be controlled when facing the problem of PM emissions because of the presence of the ultrafine component (< 100 nm) that, even though negligible in mass concentration, can cause serious health problems dominating the multimodal PM size distribution when expressed as particle number concentrations [3,4]. Consequently, a careful evaluation of the environmental impact of biofuels has to consider the formation/emission of the ultrafine particles and the possible effect of the biofuels on the chemical and morphological features of the carbon particulate matter, also enhancing its adverse effect on human health [5]. The presence of oxygen-bonded atoms into the biofuel structure modifies the oxidation pathways, generally improving carbon oxidation, in this way subtracting carbon to the growth pathways leading to the formation of high molecular mass compounds. In global or local rich conditions featuring combustion systems, however, only a partial oxidation might occur with formation of oxygenated species with high molecular mass [6] intervening in the particle formation and growth and hence affecting the particle features [7,8].

In such a framework, the present paper reports a study of the formation of combustion-generated particles produced by ethylene flames doped with butanol isomers (up to 20% of total carbon) at different equivalence ratios. In-situ optical techniques and physico-chemical diagnostics for the determination of PM particle size distributions and chemical characteristics have been used as diagnostic tools. The aromaticity and functionalities of the carbon particulate matter thermophoretically sampled were also studied in the highest equivalence ratio condition ($\varphi = 2.46$) to investigate the possible effect of butanol isomers on the morphological and

* Corresponding author.
E-mail address: mariano.sirignano@unina.it (M. Sirignano).

https://doi.org/10.1016/j.combustflame.2018.10.025

chemical features of combustion-generated particles with particular regard to the presence of oxygenated functionalities on/into soot particles.

Butanol isomers have been chosen since they represent an important source of biofuels derived from biomass and their impact on combustion characteristics and emissions has been increasingly studied as briefly summarized in the following.

1.1. Background

The main parameters (laminar flame speeds and ignition delay times) featuring butanol combustion have been already assessed in practical combustion devices as well as on lab-scale flames [9–13]. Also, kinetic schemes are currently available to describe the main reaction pathways of butanol isomers [14–16]. As regards carbon particles and their precursor formation, the butanol isomer structure has been found to be important for aromatic compound production. In low-pressure burner stabilized fuel-rich premixed flames, Oßwald et al. [13] have found that aromatic species production is enhanced by t-butanol and i-butanol significantly more than by 1- or 2-butanol. Camacho et al. [17] measured particle size distribution on burner stabilized stagnation flames comparing n- and i-butane flames with n- and i-butanol, finding an effect of the branching functionality on soot formation. McEnally and Pferfelle [18,19] studied coflow diffusion methane/air flames doped with the four butanol isomers finding a relation between fuel structure and soot propensity. These studies are generally focused on the amount, in mass and number, of particulate matter produced with butanol isomers.

Lighty's group [20] recently studied the internal structure of soot formed burning n-butanol/n-dodecane blends in a two-stage burner. The decrease of particle total volume fractions and a modification on the nanostructure of the particles produced have been observed also demonstrating that the use of butanol significantly changes the reactivity of soot and induces the presence of oxygenated functionalities on the surface of the examined samples [21].

More recently, a systematic study on the four butanol isomers has been conducted in a normal and inverse diffusion flame [22]. Specifically, all the isomers caused a noticeable reduction of the primary particle size along with a lower reactivity for the inverse diffusion flame, whereas a slight increase of the primary particles and a higher reactivity were observed for the normal diffusion flame [22].

Different butane and butanol isomers were investigated in counterflow non-premixed flame, and t-butanol was found to be the most sooting butanol isomer [23]. Butanol isomers were also added into n-heptane/toluene co-flow partially premixed flames finding the higher soot formation tendency in the case of tertiary butanol and isobutanol addition [24]. Viteri et al. [25] studied the formation of polycyclic aromatic hydrocarbons (PAH) and soot from the pyrolysis of the four butanol isomers pointing out some differences in the sooting tendencies of different isomers, namely the t-butanol having the highest one.

All these works demonstrate how the combustion configuration as well as the amount of butanol used are important to assess the role of butanols on the total amount of soot and its reactivity. For this reason, this paper is focused on the effect of butanol isomers on the production and structural properties of particulate formed in premixed flames, a flame configuration suitable for controlling and monitoring the main combustion parameters.

2. Experimental methods

Atmospheric pressure, premixed ethylene/air flames with equivalence ratios, φ, of 2.01, 2.16, 2.31, and 2.46 were stabilized on a capillary burner. The burner was cooled with recirculation water – 1 l/min – kept at 80 °C with a thermostatic bath and a steel plate was positioned at 3 cm from the burner exit to stabilize the flames. The flames so produced constituted the reference cases for studying the effect of butanol isomers on carbon particulate matter formation. The four butanol isomers (1-butanol, 2-butanol, i-butanol, and t-butanol) were added by substituting part of the ethylene (10% and 20% of the total carbon fed) to the reference ethylene/air flames. The butanols were fed by a syringe pump into the fuel stream, which was preheated to allow butanols vaporization (boiling points range from 82 °C for t-butanol to 118 °C for 1-butanol). The butanol isomers were added keeping simultaneously constant the total carbon flow rate, the equivalence ratio and the cold gas velocity by a suitable dilution with nitrogen. The same experimental setup has been previously used for studying other oxygenated fuels [7,8,26–30]. Combustion conditions are reported in Table 1.

Table 1
Flame conditions (gas flow rates are reported in SLPM – Burner diameter is 5.6 cm).

% Butanol	0	10	20
φ = 2.01; Gas velocity @STP = 10 cm/s			
Ethylene	1.82	1.64	1.46
Air	12.95	12.62	12.3
Nitrogen	0	0.41	0.83
Butanol	0	0.09	0.18
% Butanol	0%	10%	20%
φ = 2.16; Gas velocity @STP = 10 cm/s			
Ethylene	1.94	1.74	1.55
Air	12.83	12.51	12.19
Nitrogen	0	0.42	0.83
Butanol	0	0.1	0.19
% Butanol	0%	10%	20%
φ = 2.31; Gas velocity @STP = 10 cm/s			
Ethylene	2.06	1.85	1.64
Air	12.71	12.4	12.08
Nitrogen	0	0.42	0.84
Butanol	0	0.1	0.21
% Butanol	0%	10%	20%
φ = 2.46; Gas velocity @STP = 10 cm/s			
Ethylene	2.17	1.95	1.74
Air	12.6	12.28	11.97
Nitrogen	0	0.42	0.85
Butanol	0	0.11	0.22

The experimental setup for optical and particle size distribution as well as collection on quartz plate is schematized in Fig. 1. Combustion-generated particles were detected by laser induced emission (LIE) measurements in the 200–550 nm range, using as excitation source the fourth harmonic of a Nd:YAG laser at 266 nm, with the same optical set up previously used [27–29,31]. In the LIE spectra, a broad peak was distinguishable in the UV region, between 350 and 450 nm, due to Laser Induced Fluorescence (LIF). For a higher wavelength, namely at 550 nm, the signal was instead due to Laser Induced Incandescence (LII). According to previous studies, LIF signals are attributed to aromatic hydrocarbons in condensed-phase nanostructures which are not able to incandesce [3,31 and references therein]. We collected the entire spectrum and thus we could identify the C2-Swan bands and avoid the interference. It is possible that gas-phase PAH also contribute – likely in smaller wavelength part – to LIF signal. Over years LIF has been attributed to single gas-phase PAHs as well as to a generic "high molecular weight precursors" class. The proposed attribution made here does not change the validity of the discussion on the role of the isomers on the formation of the aromatic compounds and their evolution. LII signal is mainly due to solid soot particles

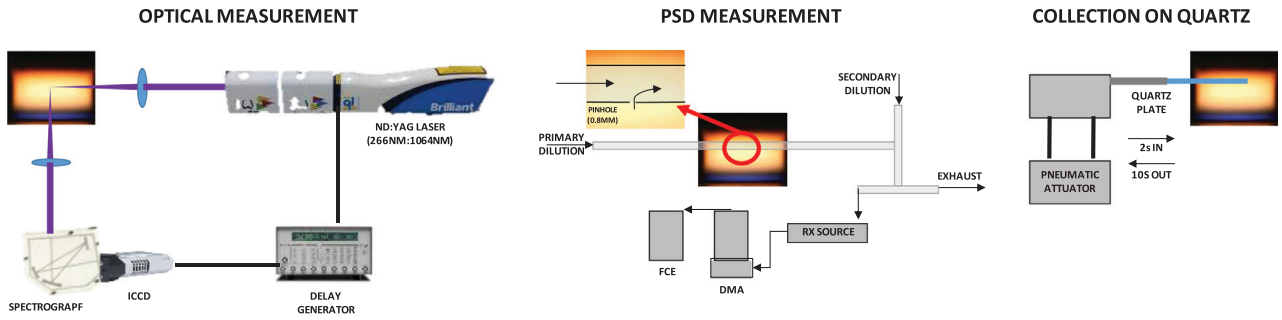

Fig. 1. Schematic representation of the diagnostic apparatus.

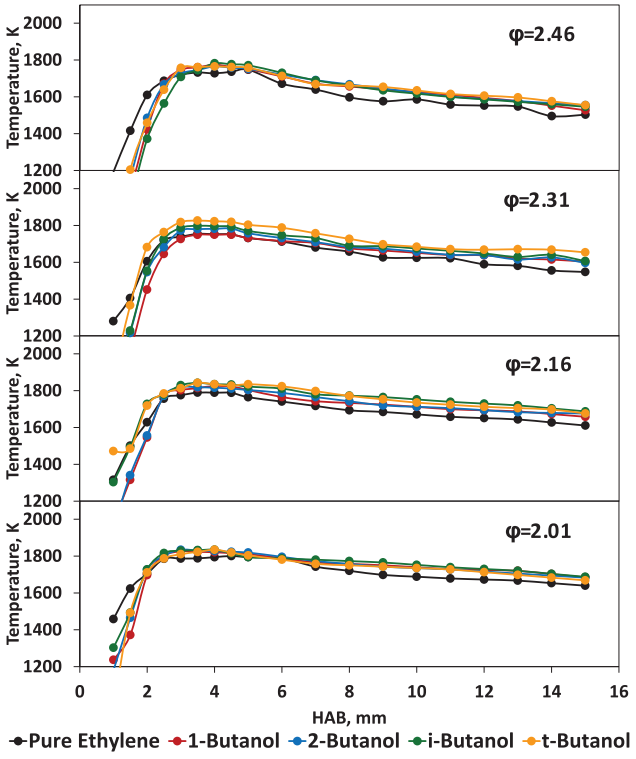

Fig. 2. Axial flame temperatures for flames doped with 20% of 1-butanol, 2-butanol, i-butanol, and t-butanol for the investigated equivalence ratios compared with pure ethylene flames.

that are able to dissipate the acquired energy by thermal emission rather than by fluorescence emission and are the main contributors to the particle volume fraction. The LII signal acquisition was delayed by 50 ns with respect to laser pulse to avoid the interference of short living fluorescence signals. For each measurement, 500 acquisitions were taken in accumulation mode: increasing the number of acquisitions, the uncertainty was not significantly reduced.

Temperature was measured by using an R-type uncoated thermocouple with a bead size of 250 µm. Measurement uncertainty is within +/− 50 K. Temperature measurements were corrected for gas radiations following the procedure of Eisner and Rosner [32]. Figure 2 reports the axial temperature profiles measured for the pure ethylene flames in all the investigated equivalence ratios in comparison with 20% butanol doped flames. It can be observed that the differences, in terms of temperature peak value and position, rely within the experimental uncertainty (±50 K and ± 0.5 mm) in all the investigated conditions. For all the flames examined, the largest temperature difference was observed at the end of the flame where the higher (lower) amount of soot formed increases (decreases) heat losses by flame radiation. Similar temperature profiles were measured for the ethylene/10% butanol flames. It is worth to note that the different adiabatic flame temperatures of the different mixtures weakly influence the measured temperatures which, instead, are mainly determined by the radiation losses and the energy balance for the specific burner. The different temperature in the preheating zone, where there is a large uncertainty due to the probe location and the steep gradient, is probably due to the different burning velocity of the alcohols.

Beside temperature and in-situ optical measurements, some analytical/spectroscopic methods were implemented on the bulk carbon particulate matter collected thermophoretically on a 75 × 25 × 1 mm quartz plate horizontally inserted in the flame for 2 s. To achieve the deposition of enough material for the structural analysis, this procedure was repeated several times, allowing for a cooling cycle at room temperature of 10 s after each insertion. The sampling procedure has been recently developed and used for the structural analysis of the carbon particulate matter collected in ethylene flames doped with 2,5-dimethylfuran [7] and ethanol [8]. Tests were performed with different numbers of insertions, showing no effect of the sampling procedure on the composition/structure of the sampled material as verified by Raman and FTIR analysis. Raman spectra were measured directly on the carbon samples deposited on the quartz plate by means of a Horiba XploRA Raman microscope system (Horiba Jobin Yvon, Japan) equipped with a frequency-doubled Nd:YAG solid-state laser ($\lambda_{max} = 532$ nm). More details on the Raman measurements and spectra acquisition are available elsewhere [7,8,33]. FTIR and UV–visible spectroscopy were applied to the carbon particulate matter samples removed from the quartz plate. FTIR spectra in the 3400–600 cm^{-1} range were acquired in the transmittance mode using a Nicolet iS10 spectrophotometer. Analyses were performed on the sample dispersions prepared by mixing and grinding the carbon particulate matter samples in KBr pellets (0.2–0.3 wt%) [34]. For the UV-visible analysis carbon particulate matter samples were suspended in N-methyl-2-pyrrolidinone (NMP, with a concentration of 10 mg/L) and analyzed in a 1-cm path length quartz cuvette using an Agilent UV–vis 8453 spectrophotometer.

Size exclusion chromatography (SEC) analysis was carried out on HP1050 high-pressure liquid chromatography (HPLC) to evaluate the size and/or molecular weight (MW) distribution of the sampled particles. Carbon samples suspended in NMP (concentration of 100 mg/L) were separated on a 30 cm × 7.5 mm outer diameter Jordi Gel divinylbenzene solid bead "nonporous" column (injection volume of 20 µL, NMP flow rate of 0.8 mL/min, and room temperature). HPLC was equipped with a diode array detector to measure online UV–vis spectra of the size/MW-segregated fractions from 250 to 600 nm. The SEC calibration curve used for the size/MW evaluation was obtained using polystyrene standards of high MW. To verify the separation efficiency for carbonaceous sam-

ples of large size/MW, a sample of commercial carbon black (N110 carbon black, Phillips Petroleum) was used. From the size (diameter) of carbon black, measured by dynamic light scattering (DLS) (Mastersizer 2000 granulometer, Malvern instrument), and considering a spherical shape and a density of 1.8 g/cm^3 an "apparent MW" was calculated [35] that fitted well with the extrapolated calibration curve of polystyrene standards. The procedure allowed verifying the effectiveness of the non-porous column to separate carbonaceous compounds as larger as soot aggregates up to the exclusion limit of 1×10^{10} u.

The experimental error for SEC and Raman, FT-IR and UV–visible spectroscopy measurements was evaluated to be less than 10%.

Particle size distribution (PSD) measurements were performed by sampling particles from the flames with a horizontal probe adopted in previous work [36–41]. The horizontal probe has been usually adopted with a single stage dilution and a quite small pinhole (<0.3 mm) that allows to have a large dilution but it is easy to be clogged in highly sooting conditions. In the setup adopted here [29,31,36], the probe has an ID = 8 mm, a wall thickness of 0.5 mm, and a pinhole diameter of 0.8 mm. A two-stage dilution system has been adopted: the carrier gas has been set to 4 Nl/min (at 273 K) as for the first dilution and to 65 Nl/min in the second dilution stage. An overall dilution of 500 is achieved for the investigated conditions with a global residence time in the probing systems of 100 ms before entering in the detection system. The PSD measurement was highly repeatable, the uncertainty of the PSD measurement mainly derives from the stability/fluctuations of the flame and hence the error bars are not reported.

For the PSD measurements, a nano-DMA was used (TapCon 3/150 DMA system in high voltage mode corresponding to a nominal size range 2–100 nm equipped with a Faraday Cup Electrometer detector). At the entrance of the DMA, particles were taken to Fuchs' steady-state charge distribution [42] by using Soft X-Ray Advanced Aerosol Neutralizer (TSI model 3088). Particles entering the nano-DMA are separated in an electrical classifier and then counted by an Electrometer Faraday Cup. By varying the electrical field applied to separate particles it is possible to rebuild the original PSD. The PSDs obtained by DMA were corrected for losses in the pinhole and the probe following the procedure reported in the literature [43–45]. DMA separates particles on the basis of their mobility diameter so that the particle diameter could be retrieved from the correlation proposed by Singh et al. [46].

3. Results and discussion

Provided the similarity of the temperature profiles for the equivalence ratios and type of butanol isomers investigated, hereafter generally named butanols, (see experimental section and Fig. 2), it is possible to compare the axial profiles of LIF and LII signals that are reported in Fig. 3 for the pure ethylene flame and ethylene/20%-butanol flames. The LIF signals (Fig. 3-top) are reported for the flames with $\varphi = 2.01$ where no LII was detected. Conversely, the LII signals (Fig. 3-bottom) are reported for flames with $\varphi = 2.46$ where the highest LII signal is measured.

LIF and LII signals exhibit the typical spectral shape (not reported) and profile measured before for ethylene flames [31] suggesting that butanols did not significantly change the process of particle inception, similarly to other biofuels [26–30]. According to previous works [3,31 and references therein], as LII signal is due to soot particles, the LIF signal has been assumed to be directly related to the concentration of condensed-phase nanostructures. The effect of butanol doping on LII signal, related to the soot particles and their aggregates, is very relevant and the reduction is as high as 80% for the t-butanol. The LIF signal appears instead to be roughly the same for all the butanol isomers; just a reduction of

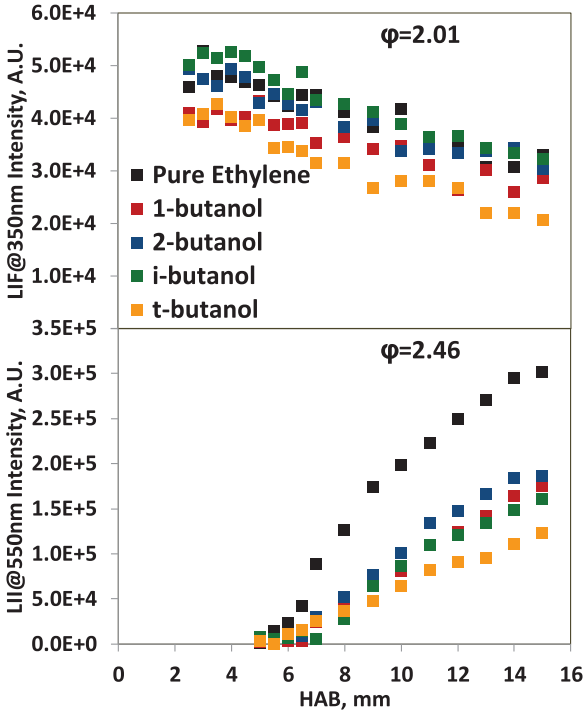

Fig. 3. Top: LIF detected along the axis of the pure ethylene (black points) and ethylene/20% butanol (colored points) flames for $\varphi = 2.01$. Bottom: LII detected along the axis of the pure ethylene (black points) and ethylene/20% butanol (colored points) flames at $\varphi = 2.46$.

about 30% of the signal is observed along the flame doped with t-butanol, and close to the flame front of the flame doped with 1-butanol. Table 2 reports the percentage variation for both LIF and LII signals measured at their maximum for all the butanol isomers. The negative variation indicates a reduction of the signal whereas the positive variation indicates an increase of the signal with the addition of butanol isomers.

The reduction of LII (soot) is consistent through all the equivalence ratios when butanols are added; t-butanol is the isomer that reduced the most the LII signal (reduced soot formation). Also, looking at the reduction obtained with 10% and 20% of butanols, it can be seen that the reduction of LII is higher as the butanol content increases for almost all the isomers, although a trend cannot be clearly distinguished for all of them. On the other hand, LIF signals are not significantly reduced – the maximum variation is within 30% and thus it is not possible to obtain a clear global trend with the butanol percentage. It is worth to underline that LIF has a large error (±15%) due to the overlapping of LII signal. However, none of the butanol isomers reduces significantly the LIF intensity.

The LII signal decrease, signature of soot formation decrease, appears to be somehow related to the oxygen bonded to the fuel carbon which is subtracted from the growth pathways. Reduction of LIF signal, whether related to condensed nanostructures or specific PAH, is less evident – within the error – since such species are related to nucleation pathways which are less inhibited by butanols doping with respect to the soot growth process similarly to what found for ethanol in similar conditions [26,27]. Soot reduction is in line with literature data for butanols [20–24]. The fact that t-butanol is the most reducing isomer is in contrast with other studies conducted in coflowing normal and inverse diffusion flame configurations [22], in pyrolysis conditions [25] and in partially premixed flames [23,24]. Overall, all the butanol isomers present a similar important effect on soot reduction whichever the combustion system configuration. In particular, the propensity of

Table 2
Percentage variation of LIF and LII signal intensity for effect of butanol isomers addition to ethylene flame. Experimental uncertainty: ± 5% for LII ± 15% for LIF.

$\varphi = 2.01$											
1-But	10%	20%	2-But	10%	20%	i-But	10%	20%	t-But	10%	20%
LIF	−4%	−12%	*LIF*	13%	7%	*LIF*	13%	13%	*LIF*	3%	−10%
LII	-	-	*LII*	-	-	*LII*	-	-	*LII*	-	-
$\varphi = 2.16$											
1-But	10%	20%	2-But	10%	20%	i-But	10%	20%	t-But	10%	20%
LIF	2%	−5%	*LIF*	14%	7%	LIF	27%	21%	*LIF*	5%	−5%
LII	−63%	−74%	*LII*	−43%	−51%	LII	−44%	−60%	*LII*	−58%	−89%
$\varphi = 2.31$											
1-But	10%	20%	2-But	10%	20%	i-But	10%	20%	t-But	10%	20%
LIF	23%	−6%	*LIF*	12%	7%	*LIF*	0%	16%	*LIF*	15%	−6%
LII	−46%	−56%	*LII*	−43%	−51%	*LII*	−41%	−60%	*LII*	−54%	−80%
$\varphi = 2.46$											
1-But	10%	20%	2-But	10%	20%	i-But	10%	20%	t-But	10%	20%
LIF	−19%	−13%	*LIF*	−7%	−13%	*LIF*	−1%	−1%	*LIF*	−13%	−13%
LII	−48%	−52%	*LII*	−34%	−39%	*LII*	−25%	−48%	*LII*	−42%	−64%

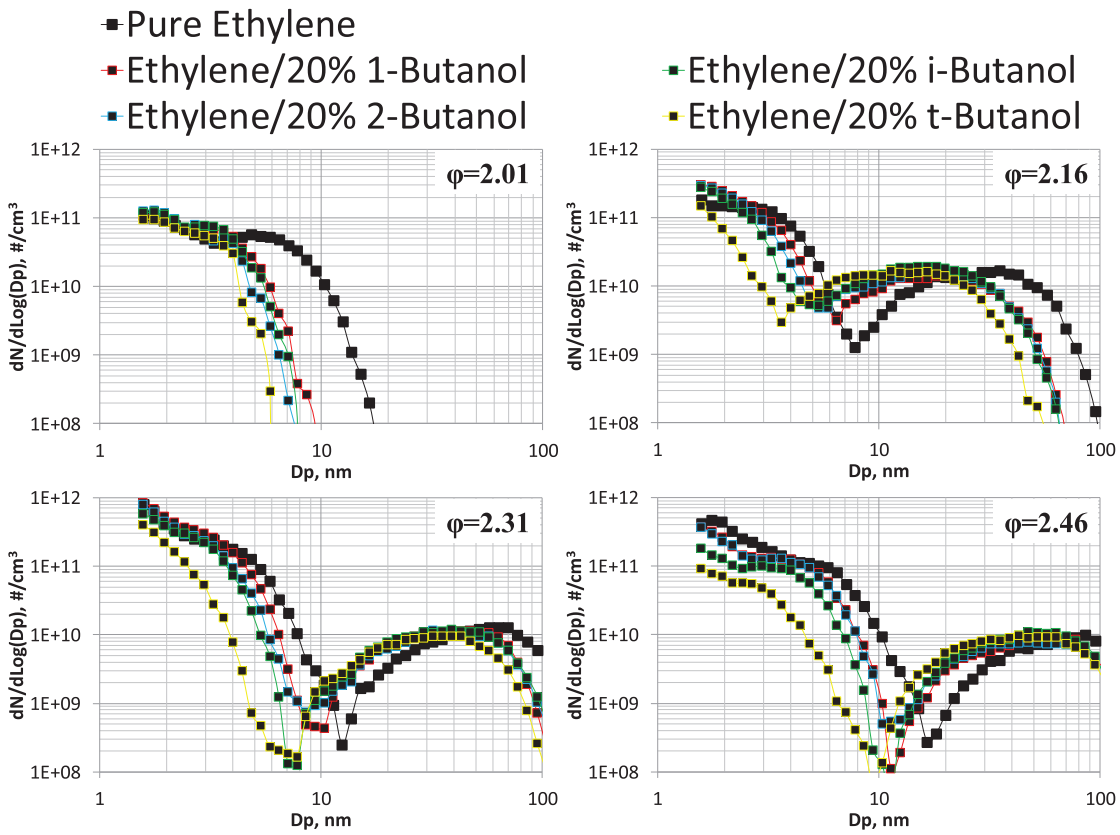

Fig. 4. PSD measured at HAB = 15 mm in the pure ethylene (black points) and ethylene/20% butanol (colored points) flames for different equivalence ratios.

t-butanol to be converted after methyl abstraction into acetone – which can be further oxidized without contributing significantly to growth process - could justify the enhanced behavior in particle reducing of t-butanol [47–51].

Besides reducing the formation of carbon particles (Fig. 3(b)), the PSDs of the particles sampled at the end of the flame (HAB = 15 mm), reported in Fig. 4, show that the addition of butanols to ethylene generally reduces the size of the formed particles for all the equivalence ratios. The shift in the PSD toward smaller sizes confirms the occurrence of a large mass reduction of carbon particles for effect of butanol content, consistently with the LII data above reported (Table 2). The number concentration of particles with sizes below 10 nm is less affected by the presence of butanols, in agreement with LIF data. In some cases, there is also a small increase, but overall the variation is much less evident. However, differently from the LIF data where the uncertainty is larger, it is also possible to observe that as the equivalence ratio increases the differences between the four isomers, and t-butanol in particular, become more evident as regards smaller particles. As can be observed in Fig. 4, the effect of butanols in the flame with $\varphi = 2.01$ is such that the shape of PSD changes from bimodal to unimodal by adding butanols. On the other side, the effect of butanols on the

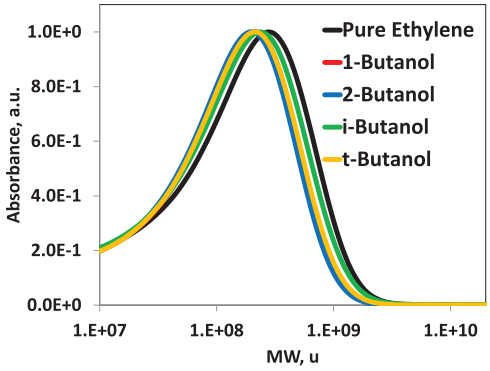

Fig. 5. MW distributions obtained by SEC of the carbon particulate matter aggregates collected on a quartz plate at 15 mm HAB and $\varphi = 2.46$ in the pure ethylene (black line) and ethylene/20%butanol (colored lines) flames.

shape of PSD is less evident for the flames with $\varphi = 2.46$ where the bimodality is evident for all the isomers. In fact, the ethylene flame with $\varphi = 2.01$ is close to the sooting limit, i.e. to the appearance of the second mode in the PSD featuring soot particles and aggregates, hence small changes in the gas-phase PAH and radical pool are sufficient to cause a significant change of the PSD. On the other side, the flame with $\varphi = 2.46$ is in fully-sooting regime, in this latter flame the effect of butanols addition is rather mitigated. Also looking at the trend reported in Table 2 and in Fig. 4, the percentage reduction of the total particulate (LII) decreases as the equivalence ratio increases, suggesting that the butanol isomers are less effective in particle reduction. This behavior can be linked to a direct effect of butanols onto the formation of PAH – similarly to what found for other alcohols and ethanol [26,27] - which turns into a large effect on PSD shape in flame conditions in which the formation process is dominated or largely influenced by nucleation process (equivalence ratio close to 2). As the equivalence ratio increases, the nucleation process is dominated by surface growth, mainly by acetylene, and consequently less affected by the butanols content. This interpretation could be generally extended to whichever alcohol as inferred on the basis of a similar finding observed for ethanol addition [26,27].

A detailed compositional and spectroscopic characterization of the samples thermophoretically collected has been performed to verify the occurrence of butanol effect on particulate characteristics. The analysis has been carried out for the $\varphi = 2.46$ flames where large amounts of carbonaceous material could be collected for the following analyses. Before analyzing the spectroscopic properties of the soot sampled in flames doped with different butanol isomers, SEC analysis has been performed to evaluate the occurrence of size changes. Figure 5 reports the SEC chromatograms zoomed in the molecular-weight zone of interest of soot aggregates. Carbon particulate matter sampled in flames doped with butanols shows generally a smaller mode size, however the differences can be considered small and allow performing a direct comparison of the structural properties of samples.

Raman spectroscopy has been used to characterize the level of aromaticity of particles sampled using different butanols. Figure 6 (top) reports Raman spectra measured for the particles sampled in the investigated conditions. No significant differences can be noticed, clearly suggesting that the aromaticity of the particle structure produced in all the doped flames is not changed. By contrast, for other oxygenated fuels, i.e. ethanol, the reduction of the total amount of particulate was found to be accompanied by a significant change in morphology and aromaticity of the particles produced [8]. The similarity of the samples collected with different butanols is confirmed by the similarity of the UV-visible mass ab-

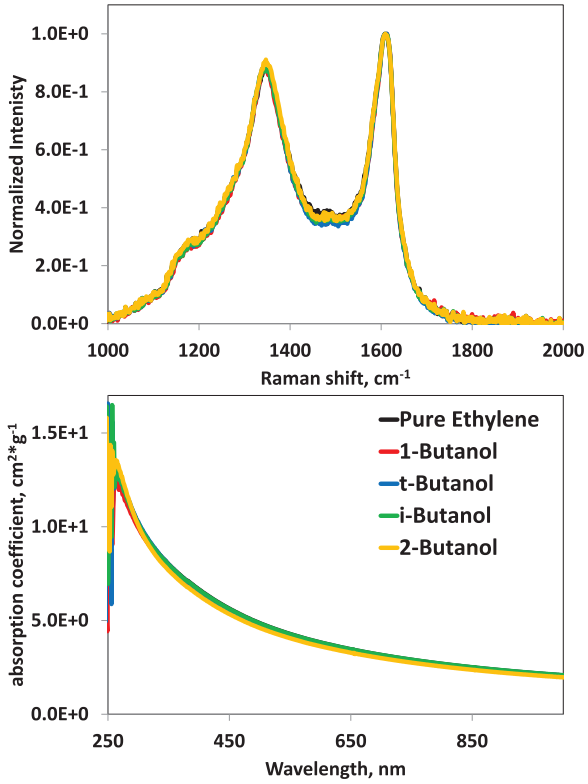

Fig. 6. Raman spectra (top) and absorption spectra (bottom) measured for the samples collected on a quartz plate at 15 mm HAB and $\varphi = 2.46$ in the ethylene (black line) and ethylene/20% butanol (colored lines) flames.

sorption coefficients reported in Fig. 6 (bottom) in the 250–900 nm range. It is worth to remind that the spectroscopic analysis has been performed on the raw carbon particulate matter samples. In particular, Raman spectra were measured directly on the quartz plate while UV–vis analysis has been performed on NMP suspension of known concentration of carbon particulate matter removed from the quartz plate.

Finally, to verify the presence of oxygen-containing functionalities on carbon particles, FTIR spectroscopy has been adopted due to its capability to identify the functional groups present on the particle surface [34]. FTIR spectra of carbon samples collected in the ethylene (black line) and ethylene/20% butanol (colored line) flames with $\varphi = 2.46$ are reported in Fig. 7. The spectra have been collected using the same conditions, i.e., the same carbon concentration within KBr disk and disk thickness, to direct compare the results. More details on the sample preparation for FTIR measurements are available elsewhere [34]. The spectra reported in Fig. 7 are focused in the zone where oxygen functionalities can be detected. Differently from the other spectroscopic analysis, differences between the particles sampled in the reference ethylene flame and those collected in the ethylene/20% butanols flames can be noticed.

The FTIR spectral region 4000–2500 cm^{-1} is generally attributed to OH stretching peaks (alcoholic groups around 3500 cm^{-1}), and thus is the first evidence of the larger presence of oxygenated functionalities in the samples produced in t-butanol and the 1-butanol-doped flames. This increase cannot be linked with the presence of water on the surface since the particulate samples have been carefully dried for 72 h before performing the analysis. Considered the same drying procedure and the similarity of aggregate sizes, these differences can be attributed to a different OH content. It has to be underlined that the absorption intensity of OH group is almost ten times higher than that of aromatic hydro-

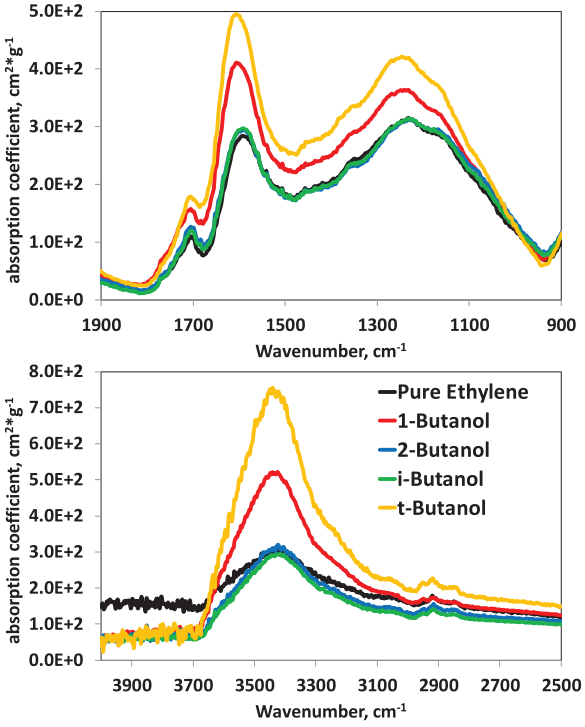

Fig. 7. Infrared mass absorption coefficients of soot particles sampled at 15 mm HAB and $\varphi = 2.46$ in the ethylene (black line) and ethylene/20% butanol (colored line) flames in the (top) 900–1900 cm^{-1} and (bottom) 2500–4000 cm^{-1} wavenumber ranges. The spectra reported have been obtained after subtraction of the continuum.

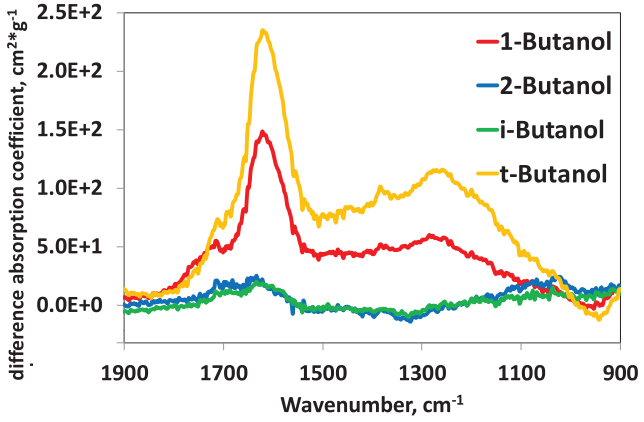

Fig. 8. Difference between the infrared mass absorption coefficients in the 900–1900 cm^{-1} wavenumber range of carbon particulate matter at 15 mm HAB and $\varphi = 2.46$ in the ethylene/20% butanols flames and pure ethylene.

gen, thus a small difference of OH content is clearly visible as implies large FTIR signal differences. The interpretation of the spectral differences in the 1900–900 cm^{-1} region (Fig. 7, bottom) is far more complex: it can be observed that the mass absorption coefficients between 900 and 1300 cm^{-1} and at 1600 cm^{-1} are higher for the particles sampled in t-butanol and the 1-butanol-doped flames.

The differences in the FTIR signal intensity are better shown in Fig. 8 reporting the spectra obtained as difference between the infrared mass absorption coefficients of carbon particulate of ethylene/20% butanols flames and those of the pure ethylene flame. The higher intensity of the 1600 cm^{-1} peak, due to the C = C stretching mode of polyaromatic systems, is clearly visible for 1-butanol and t-butanol. The 1600 cm^{-1} peak is typically reinforced by the irregularity/dissymmetry of the aromatic moiety caused by whichever

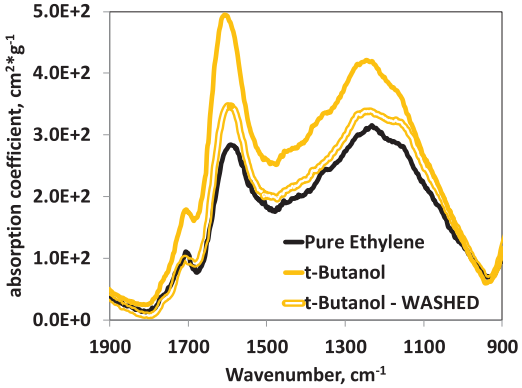

Fig. 9. Infrared mass absorption coefficients in the 900–1900 cm^{-1} wavenumber range of soot particles produced at 15 mm HAB and $\varphi = 2.46$ in the pure ethylene (black solid line) and ethylene/20% t-Butanol flame before (solid yellow line) and after (empty yellow line) washing the samples with DCM.

kind of ring substitution. In particular, the increase in the dipole moment associated with ring vibrations in the presence of oxygen enhances the intensity of the C = C stretching peak [52,53].

In the 1-butanol and t-butanol soot sample also a higher intensity of the 1720 cm^{-1} absorption peak can be noticed, most likely due to the stretching of ketonic and/or esteric C = O groups [54]. Finally, the higher absorption in the 1300–1000 cm^{-1} range for 1-butanol and t-butanol soot could be associated to other oxygen functionalities as ether type structures (C–O–C) [54] rather than to a higher aromatic content. It is worth to remind that the aromaticity of all the samples has been evaluated by both Raman and UV–vis spectroscopy and has been found to be quite similar. No significant differences in terms of aromatic hydrogen content evaluated on the basis of the intensity of the out of plane aromatic hydrogen bending peaks (900–700 cm^{-1}) were found, differently from our previous studies on 2,5-dimethylfuran and ethanol doped flames. This is probably due to the different molecular structure of the biofuels studied. In the case of butanols indeed it seems that oxygenated functionalities are not embedded inside the aromatic network. To confirm this result t-butanol particulate, showing the most intense FTIR difference in comparison to ethylene particulate, was washed with dichloromethane in order to remove the soluble organic fraction. The mass absorption coefficients of carbon particulate collected in the ethylene and in the t-butanol flame, before and after DCM washing, are reported in Fig. 9. After the soluble organic fraction removal, the infrared spectrum of t-butanol particulate becomes more similar to that of ethylene. This is an indication that the oxygenated functionalities could be mainly addressed to gas-phase oxy-PAH and/or condensed-phase nanostructures included in the carbon particulate matter.

Hereon an analysis of the collected results and a possible explanation for the effect of the different butanol isomers are proposed. It is worth to remind that the data presented here are collected in quite different conditions from those available in literature in terms of pressure and flame configurations. Also at the present gas phase analysis is not available and a complete kinetic modeling was not performed hence it is not possible to furnish detailed kinetic analysis. Most of the considerations are derived from other kinetic works on butanols in different conditions and for other biofuels in the same flame configuration [26,27].

By substituting butanols to ethylene in the fuel mixture, the presence of oxygen-borne atoms favors a better oxidation of the fuel molecules subtracting carbon to the growth pathways leading to the formation of benzene and gas phase PAH [15]. It is worth to remind that in the investigated conditions the equivalence ratio has been kept constant, so that the role of oxygen atoms is to

favor kinetically the oxidation process of fuel molecules since the overall amount of oxygen available did not change. The effect of oxygenated fuel on the main oxidation pathways and their role in reducing the net carbon contributing to the growth pathways are well accepted. The reduced formation of PAHs and first particles is quite evident at the soot particle formation threshold ($\varphi = 2.01$), where the nucleation is the dominant process. As the equivalence ratio increases, the effect is reduced since surface growth takes place and is less affected by the butanol doping - the acetylene should not be significantly reduced by the use of butanols added as 20% of total carbon.

The effect of t-butanol seems to be more evident than other biofuels investigated under similar conditions. In fact, there is a slowdown of the carbon growth process, as demonstrated by the reduced formation of the large molecules and small particles (LIF and PSD) and finally of large soot aggregates (LII and PSD) on which the t-butanol seems to be the most effective. According to what already stated generically for alcohols, this enhanced effect should be linked with the presence of most effective oxidation pathways for t-butanol. It has to be considered that this effect is in contrast with that found in other studies – in other conditions – where the t-butanol is the less effective in reducing particulate matter. The dependence in particle reduction of biofuels on the flame configurations has been found also for other fuels. Ethanol [26,27], Dimethyl ether [28], and furans [29,30], at 10–20% have been found to even increase the formation of particles in opposed flow diffusion flames configuration and have a significant reducing effect in premixed flame configuration, similar to what adopted in this work. The most effective oxidation pathways for t-butanol has to be considered specifically for the proposed conditions. In fact, the observed behavior of t-butanol could be due to the particular combustion conditions investigated; in pyrolytic conditions the formation of tertiary radical could favor the growth process and the t-butanol would be the less effective in reducing the particulate formation, such as found by other groups [22,25]. Looking at the kinetic studies of Moos et al. [47], Veloo et al. [48], Jin et al. [49], Lefkowitz et al. [50] Sarathy et al. [51], they all agree that part of the t-butanol is converted into acetone after methyl abstraction – which can be further oxidized without contributing significantly to growth process. The amount of t-butanol converted in acetone with respect to other products as isobutene and propen-2-ol is depending on the conditions investigated. This pathway could be enhanced in the conditions investigated in this work justifying the enhanced behavior in particle reducing of t-butanol.

Further investigations are needed to obtain a general consideration on the differences between the four butanol isomers. However, the significant effect of t-butanol in slowing down the growth process, at least in the investigated conditions, turns also into the formation of oxygenated compounds with high molecular weight. These compounds are negligible in terms of mass, however their contribution to mark the chemical features of the total particulate matter produced during t-butanol combustion appears evident. The nature of these oxygenated compounds with high molecular weight is actually under investigation, and, although oxy-PAHs [55–58] are being largely considered, a conclusive proof is not found yet.

4. Conclusions

In this work, a systematic study of the effect of the four butanol isomers on the formation of combustion-generated particles as well as on their morphology, aromaticity, and functionalities has been conducted. Butanol isomers were fed as substituent up to 20% of the total carbon to premixed ethylene/air flames with different equivalence ratios, namely $\varphi = 2.01$, 2.16, 2.31, 2.46. Combustion parameters such as carbon flow rate, cold gas velocity and equivalence ratio were kept constant with butanols doping to allow a direct comparison and isolate the effect of the fuel structure.

In all the investigated conditions, butanol isomers significantly reduced the total amount and the size of soot particles (tracked by LII and PSD) whereas have less, and in some conditions any effect on condensed-phase nanostructures (tracked by LIF and PSD). This effect is similar to what found in quite similar combustion configurations for other oxygenated fuels such as ethanol, dimethyl ether and furans. Among the isomers, t-butanol seems to be the most reducing one, although literature data for butanols mixed with long-chain alkanes (n-heptane, n-dodecane) and diesel surrogates report different trends for the isomers indicating t-butanol as the less effective in reducing the particle formation.

Particles generated by ethylene and ethylene/butanol isomers have the same characteristics in terms of size and aromaticity (UV–visible and Raman spectroscopy). Conversely, from FTIR analysis, the highest presence of oxygen bonded to carbon atoms in the particulate matter generated in the ethylene flames doped with butanols was found. The particles sampled from 1-butanol and t-butanol flames contain many functionalities, e.g., C=O, C–O-C and OH, suggesting the intervention of oxygenated compound in the particulate formation. Most of the oxygen functionalities were lost after washing in dichloromethane, i.e. after the removal from soot particles of small particles and/or high-molecular mass aromatic molecules.

Acknowledgments

The authors thank the European Union's Horizon 2020 research and innovation program for the financial support to the project Waste2Fuel (grant agreement No 654623).

References

[1] K. Kohse-Höinghaus, P. Oßwald, T.A. Cool, T. Kasper, N. Hansen, F. Qi, C.K. Westbrook, P.R. Westmoreland, Biofuel combustion chemistry: from ethanol to biodiesel, Angew. Chem. Int. Ed. 49 (21) (2010) 3572–3597.
[2] M. Lapuerta, O. Armas, J. Rodríguez-Fernández, Effect of biodiesel fuels on diesel engine emissions, Prog. Energy Combust. Sci. 34 (2) (2008) 198–223.
[3] A. D'Anna, Combustion-formed nanoparticles, Proc. Combust. Inst. 32 (2009) 593–613.
[4] H. Wang, Formation of nascent soot and other condensed-phase materials in flames, Proc. Combust. Inst. 33 (2011) 41–67.
[5] G. De Falco, C. Cola, M. Terlizzi, A. Popolo, M. Pecoraro, M. Commodo, M. Minutolo, M. Sirignano, A. D'Anna, R.P. Aquino, A. Pinto, A. Molino, R. Sorrentino, Chronic obstructive pulmonary disease (COPD)-derived circulating cells release IL-18 and IL-33 under ultrafine particulate (UFP) matter exposure in a caspase-1/8-independent manner, Front. Immunol. 8 (2017) 1415 OCT.
[6] C. Guan, C.S. Cheung, X. Li, Z. Huang, Effects of oxygenated fuels on the particle-phase compounds emitted from a diesel engine, Atmos. Pollut. Res. 8 (2) (2017) 209–220.
[7] C. Russo, A. D'Anna, A. Ciajolo, M. Sirignano, Analysis of the chemical features of particles generated from ethylene and ethylene/2,5 dimethyl furan flames, Combust. Flame 167 (2016) 268–273.
[8] M. Sirignano, A. Ciajolo, A. D'Anna, C. Russo, Chemical features of particles generated in an ethylene/ethanol premixed flame, Energy Fuels 31 (3) (2017) 2370–2377.
[9] X. Gu, Z. Huang, S. Wu, Q. Li, Laminar burning velocities and flame instabilities of butanol isomers–air mixtures, Combust. Flame 157 (12) (2010) 2318–2325.
[10] B.W. Weber, K. Kumar, Y. Zhang, C.J. Sung, Autoignition of n-butanol at elevated pressure and low-to-intermediate temperature, Combust. Flame 158 (5) (2011) 809–819.
[11] D.M. Karwat, S.W. Wagnon, P.D. Teini, M.S. Wooldridge, On the chemical kinetics of n-butanol: ignition and speciation studies, J. Phys. Chem. A 115 (19) (2011) 4909–4921.
[12] P. Dagaut, S.M. Sarathy, M.J. Thomson, A chemical kinetic study of n-butanol oxidation at elevated pressure in a jet stirred reactor, Proc. Combust. Inst. 32 (1) (2009) 229–237.
[13] P. Oßwald, H. Güldenberg, K. Kohse-Höinghaus, B. Yang, T. Yuan, F. Qi, Combustion of butanol isomers–a detailed molecular beam mass spectrometry investigation of their flame chemistry, Combust. Flame 158 (1) (2011) 2–15.
[14] G. Black, H.J. Curran, S. Pichon, J.M. Simmie, V. Zhukov, Bio-butanol: combustion properties and detailed chemical kinetic model, Combust. Flame 157 (2) (2010) 363–373.
[15] A. Frassoldati, R. Grana, T. Faravelli, E. Ranzi, P. Oßwald, K. Kohse-Höinghaus, Detailed kinetic modeling of the combustion of the four butanol isomers in premixed low-pressure flames, Combust. Flame 159 (7) (2012) 2295–2311.

[16] P.S. Veloo, Y.L. Wang, F.N. Egolfopoulos, C.K. Westbrook, A comparative experimental and computational study of methanol, ethanol, and n-butanol flames, Combust. Flame 157 (2010) 1989–2004.
[17] J. Camacho, S. Lieb, H. Wang, Evolution of size distribution of nascent soot in n-and i-butanol flames, Proc. Combust. Inst. 34 (2013) 1853–1860.
[18] C.S. McEnally, L.D. Pfefferle, Fuel decomposition and hydrocarbon growth processes for oxygenated hydrocarbons: butyl alcohols, Proc. Combust. Inst. 30 (2005) 1363–1370.
[19] C.S. McEnally, L.D. Pfefferle, Sooting tendencies of oxygenated hydrocarbons in laboratory-scale flames, Environ. Sci. Technol. 45 (2011) 2498–2503.
[20] H. Ghiassi, P. Toth, J.S. Lighty, Sooting behaviors of n-butanol and n-dodecane blends, Combust. Flame 161 (2014) 671–679.
[21] I.C. Jaramillo, C.K. Gaddam, R.L. Vander Wal, C.H. Huang, J.D. Levinthal, J.S. Lighty, Soot oxidation kinetics under pressurized conditions, Combust. Flame 161 (2014) 2951–2965.
[22] Y. Ying, D. Liu, Effects of butanol isomers additions on soot nanostructure and reactivity in normal and inverse ethylene diffusion flames, Fuel 205 (2017) 109–129.
[23] P. Singh, C.J. Sung, PAH formation in counterflow non-premixed flames of butane and butanol isomers, Combust. Flame 170 (2016) 91–110.
[24] B. Chen, X. Liu, H. Liu, H. Wang, D.C. Kyritsis, M. Yao, Soot reduction effects of the addition of four butanol isomers on partially premixed flames of diesel surrogates, Combust. Flame 177 (2017) 123–136.
[25] F. Viteri, S. Gracia, A. Millera, R. Bilbao, M.U. Alzueta, Polycyclic aromatic hydrocarbons (PAHs) and soot formation in the pyrolysis of the butanol isomers, Fuel 197 (2017) 348–358.
[26] M. Salamanca, M. Sirignano, M. Commodo, P. Minutolo, A. D'Anna, The effect of ethanol on the particle size distributions in ethylene premixed flames, Exp. Therm. Fluid Sci. 43 (2012) 71–73.
[27] M. Salamanca, M. Sirignano, A. D'Anna, Particulate formation in premixed and counter-flow diffusion ethylene/ethanol flames, Energy Fuels 26 (2012) 6144–6152.
[28] M. Sirignano, M. Salamanca, A. D'Anna, The role of dimethyl ether as substituent to ethylene on particulate formation in premixed and counter-flow diffusion flames, Fuel 126 (2014) 256–262.
[29] M. Conturso, M. Sirignano, A. D'Anna, Effect of furanic biofuels on particles formation in premixed ethylene–air flames: an experimental study, Fuel 175 (2016) 137–145.
[30] M. Conturso, M. Sirignano, A. D'Anna, Effect of furans on particle formation in diffusion flames: an experimental and modeling study, Proc. Combust. Inst. 36 (2017) 985–992.
[31] M Sirignano, D. Bartos, M. Conturso, M. Dunn, A. D'Anna, A.R. Masri, Detection of nanostructures and soot in laminar premixed flames, Combust. Flame 176 (2017) 299–308.
[32] A.D. Eisner, D.E. Rosner, Experimental studies of soot particle thermophoresis in nonisothermal combustion gases using thermocouple response techniques, Combust. Flame 61 (1985) 153–166.
[33] C. Russo, A. Ciajolo, Effect of the flame environment on soot nanostructure inferred by Raman spectroscopy at different excitation wavelengths, Combust. Flame 162 (2015) 2431–2441.
[34] C. Russo, F. Stanzione, A. Tregrossi, A. Ciajolo, Infrared spectroscopy of some carbon-based materials relevant in combustion: qualitative and quantitative analysis of hydrogen, Carbon 74 (2014) 127–138.
[35] A. D'Anna, A. Ciajolo, M. Alfè, B. Apicella, A. Tregrossi, Effect of fuel/air ratio and aromaticity on the molecular weight distribution of soot in premixed n-heptane flames, Proc. Combust. Inst. 32 (2009) 803–810.
[36] M. Sirignano, A. D'Anna, Coagulation of combustion generated nanoparticles in low and intermediate temperature regimes: an experimental study, Proc. Combust. Inst. 34 (2013) 1877–1884.
[37] B. Zhao, Z. Yang, M.V. Johnston, H. Wang, A.S. Wexler, M. Balthasar, M. Kraft, Measurement and numerical simulation of soot particle size distribution functions in a laminar premixed ethylene-oxygen-argon flame, Combust. Flame 133 (2003) 173–188.
[38] M.M. Maricq, Size and charge of soot particles in rich premixed ethylene flames, Combust. Flame 137 (2004) 340–350.
[39] B. Zhao, Z. Yang, Z. Li, M.V. Johnston, H. Wang, Particle size distribution function of incipient soot in laminar premixed ethylene flames: effect of flame temperature, Proc. Combust. Inst. 30 (2005) 1441–1448.
[40] M. Thierley, H.H. Grotheer, M. Aigner, Z. Yang, A. Abid, B. Zhao, H. Wang, On existence of nanoparticles below the sooting threshold, Proc. Combust. Inst. 31 (2007) 639–647.
[41] L.A. Sgro, A. De Filippo, G. Lanzuolo, A. D'Alessio, Characterization of nanoparticles of organic carbon (NOC) produced in rich premixed flames by differential mobility analysis, Proc. Combust. Inst. 31 (2007) 631–638.
[42] G.P. Reischl, J.M. Mäkelä, R. Karch, J. Neeid, Bipolar charging of ultrafine particles in the size range below 10 nm, J. Aerosol Sci. 27 (1996) 931–949.
[43] P. Minutolo, A. D'Anna, A. D'Alessio, On detection of nanoparticles below the sooting threshold, Combust. Flame 152 (2008) 287–292.
[44] L.A. Sgro, A. D'Anna, P. Minutolo, Charge distribution of incipient flame-generated particles, Aerosol. Sci. Technol. 44 (2010) 651–662.
[45] W.C. Hinds, Aerosol technology: properties, behavior and measurement of airborne particles, Wiley, New York, 1982, p. 163.
[46] J. Singh, R.I. Patterson, M. Kraft, H. Wang, Numerical simulation and sensitivity analysis of detailed soot particle size distribution in laminar premixed ethylene flames, Combust. Flame 145 (2006) 117–127.
[47] J.T. Moss, A.M. Berkowitz, M.A. Oehlschlaeger, J. Biet, V. Warth, P.-A. Glaude, F. Battin-Leclerc, An experimental and kinetic modeling study of the oxidation of the four isomers of butanol, J. Phys. Chem. A 112 (2008) 10843–10855.
[48] P.S. Veloo, F.N. Egolfopoulos, Flame propagation of butanol isomers/air mixtures, Proc. Combust. Inst. 33 (2011) 987–993.
[49] H. Jin, J. Cai, G. Wang, Y. Wang, Y. Li, J. Yang, Z. Cheng, W. Yuan, F. Qi, A comprehensive experimental and kinetic modeling study of tert-butanol combustion, Combust. Flame 169 (2016) 154–170.
[50] J.K. Lefkowitz, J.S. Heyne, S.H. Won, S. Dooley, H.H. Kim, F.M. Haas, S. Jahangirian, F.L. Dryer, Y. Ju, A chemical kinetic study of tertiary-butanol in a flow reactor and a counterflow diffusion flame, Combust. Flame 159 (2012) 968–978.
[51] S.M. Sarathy, S. Vranckx, K. Yasunaga, M. Mehl, P. Oßwald, W.K. Metcalfe, C.K. Westbrook, W.J. Pitz, K. Kohse-Höinghaus, R.X. Fernandes, H.J. Curran, A comprehensive chemical kinetic combustion model for the four butanol isomers, Combust. Flame 159 (2012) 2028–2055.
[52] C. Russo, A. Tregrossi, A. Ciajolo, Dehydrogenation and growth of soot in premixed flames, Proc. Combust. Inst. 35 (2015) 1803–1809.
[53] E. Fuente, J.A. Menéndez, M.A. Díez, D. Suárez, M.A. Montes-Morán, Infrared spectroscopy of carbon materials: a quantum chemical study of model compounds, J. Phys. Chem. B 107 (2003) 6350–6359.
[54] M.S. Akhter, A.R. Chughtai, D.M. Smith, The structure of hexane soot I: spectroscopic studies, Appl. Spectrosc. 39 (1985) 143–153.
[55] P. Elvati, A. Violi, Homo-dimerization of oxygenated polycyclic aromatic hydrocarbons under flame conditions, Fuel 222 (2018) 307–311.
[56] K.O. Johansson, T. Dillstrom, M. Monti, F. El Gabaly, M.F. Campbell, P.E. Schrader, D.M. Popolan-Vaida, N.K. Richards-Henderson, K.R. Wilson, A. Violi, H.A. Michelsen, Formation and emission of large furans and oxygenated hydrocarbons from flames, Proc. Natl. Acad. Sci. 113 (2016) 8374–8379.
[57] M. Commodo, A. D'Anna, G. De Falco, R. Larciprete, P. Minutolo, Illuminating the earliest stages of the soot formation by photoemission and Raman spectroscopy, Combust. Flame 181 (2017) 188–197.
[58] M. Commodo, G. De Falco, R. Larciprete, A. D'Anna, P. Minutolo, On the hydrophilic/hydrophobic character of carbonaceous nanoparticles formed in laminar premixed flames, Exp. Therm. Fluid Sci. 73 (2016) 56–63.